RSC Advances

PAPER

View Article Online
View Journal | View Issue

Cite this: *RSC Adv.*, 2022, **12**, 14246

Combinatorial effects of non-thermal plasma oxidation processes and photocatalytic activity on the inactivation of bacteria and degradation of toxic compounds in wastewater†

A. Raji,*[a] D. Vasu,[a] K. Navaneetha Pandiyaraj,[b] Rouba Ghobeira,[c] Nathalie De Geyter,[c] Rino Morent,[c] Vandana Chaturvedi Misra,[d] S. Ghorui,[d] M. Pichumani,[e] R. R. Deshmukh[f] and Mallikarjuna N. Nadagouda[g]

The simultaneous presence of hazardous chemicals and pathogenic microorganisms in wastewater is tremendously endangering the environment and human health. Therefore, developing a mitigation strategy for adequately degrading toxic compounds and inactivating/killing microorganisms is urgently needed to protect ecosystems. In this paper, the synergetic effects of the photocatalytic activity of TiO_2 and Cu–TiO_2 nanoparticles (NPs) and the oxidation processes of non-thermal atmospheric pressure plasma (NTAPP) were comprehensively investigated for both the inactivation/killing of common water contaminating bacteria (*Escherichia coli* (*E. coli*)) and the degradation of direct textile wastewater (DTW). The photocatalytic NPs were synthesized using the hydrothermal method and further characterized employing field emission scanning electron microscopy (FESEM), X-ray diffraction (XRD), ultraviolet-visible diffuse reflection spectroscopy (UV-Vis DRS) and photoluminescence (PL). Results revealed the predominant presence of the typical anatase phase for both the flower-like TiO_2 and the multipod-like Cu–TiO_2 structures. UV-Vis DRS and PL analyses showed that the addition of Cu dopants reduced the bandgap and increased oxygen defect vacancies of TiO_2. The inactivation of *E. coli* in suspension and degradation of DTW were then examined upon treating the aqueous media with various plasma alone and plasma/NPs conditions (Ar plasma, Ar + O_2 plasma and Ar + N_2 plasma, Ar plasma + TiO_2 NPs and Ar plasma + Cu–TiO_2 NPs). Primary and secondary excited species such as $OH^{\bullet}$, O, H and N_2* generated in plasma during the processes were recognized by *in situ* optical emission spectrometry (OES) measurements. Several other spectroscopic analyses were further employed to quantify some reactive oxygen species (ROS) such as OH, H_2O_2 and O_3 generated during the processes. Moreover, the changes in the pH and electrical conductivity (EC) of the solutions were also assessed. The inactivation of bacteria was examined by the colony-forming unit (CFU) method after plating the treated suspensions on agar, and the degradation of organic compounds in DTW was further validated by measuring the total organic carbon (TOC) removal efficiency. All results collectively revealed that the combinatorial plasma-photocatalysis strategy involving Cu–TiO_2 NPs and argon plasma jet produced higher concentrations of ROS and proved to be a promising one-step wastewater treatment effectively killing microorganisms and degrading toxic organic compounds.

Received 24th December 2021
Accepted 11th April 2022

DOI: 10.1039/d1ra09337a

rsc.li/rsc-advances

[a]*Research Division of Plasma Processing (RDPP), Department of Physics, Sri Shakthi Institute of Engineering and Technology, Coimbatore, 641062, India. E-mail: raaji.arumugam@gmail.com; Tel: +91-8012097173*

[b]*Department of Physics, Sri Ramakrishna Mission Vidyalaya College of Arts and Science, Coimbatore-641020, India*

[c]*Research Unit Plasma Technology (RUPT), Department of Applied Physics, Faculty of Engineering and Architecture, Ghent University, Ghent, 9000, Belgium*

[d]*Laser and Plasma Technology Division, Bhabha Atomic Research Centre, Trombay, Mumbai-400085, India*

[e]*Department of Nanoscience and Technology, Sri Ramakrishna Engineering College, Coimbatore-641022, India*

[f]*Department of Physics, Institute of Chemical Technology, Matunga, Mumbai, India*

[g]*Department of Mechanical and Materials Engineering, Wright State University, Dayton, Ohio 45435, USA*

† Electronic supplementary information (ESI) available. See https://doi.org/10.1039/d1ra09337a

1. Introduction

The scientific community is increasingly concerned by the dangerous contamination of the aqueous environment by a wide range of microorganisms, including bacteria, protozoa, and viruses responsible for spreading various waterborne diseases to human beings. According to the World Health Organization (WHO), 80% of the reported diseases are caused by drinking contaminated water, and 50% of child deaths result from waterborne diseases.[1] Pathogenic microbes found in water can cause infectious (*e.g.*, measles and flu) and non-infectious (*e.g.*, heart diseases and cancer) diseases.[2,3] For instance, coliform bacteria have frequently been the cause of diarrhea, cramps, fever, nausea, fatigue, *etc.*[4] Next to the high burden of microbes, the simultaneous presence of hazardous chemicals in wastewater resulting from improper industrial effluent disposal affects the environment and human health significantly.[5] The exposure of humans to toxic chemicals can trigger carcinogenesis, genetic defects, reproductive abnormalities, central nervous system degeneration, and reduced life expectancy.[6–8] Moreover, chemicals escaping into the environment can disrupt the natural balance of indigenous microbial populations and affect the aquatic flora. Hence, a mitigation strategy for adequately degrading hazardous compounds and inactivating microorganisms is urgently needed to protect ecosystems. Water disinfection methods such as ozonation and chlorination have been conventionally adopted for the inactivation of microbes.[9] Nonetheless, several drawbacks have emerged regarding these traditional treatments that engender the generation of potentially toxic by-products such as haloacetic acids and trihalomethanes upon interaction with halide ions and natural organic matter. Moreover, conventional technologies (adsorption, membrane filtration, coagulation, *etc.*) used for effluent treatment generate secondary solid waste and only partially degrade the present organic pollutants.[10] In order to overcome these problems, advanced oxidation processes (AOPs) constitute an effective alternative method concurrently acting as a disinfection technology for the inactivation of microbes and a decomposition pathway of recalcitrant organic pollutants existing in wastewater.[11] In fact, AOPs generate reactive oxygen species (ROS) and reactive nitrogen species (RNS) such as H_2O_2, OH, O, NO_2^- and NO_3^- that cause the degradation of organic pollutants into smaller non-toxic molecules and the killing/inactivation of microorganisms *via* different signaling pathways.[12–15] Those pathways trigger, amongst others, the damage of the cell membrane/wall (peptidoglycans), DNA structure and intracellular proteins. Among the numerous AOPs, non-thermal atmospheric pressure plasma (NTAPP) is distinguished, in addition to its high ability to produce ROS and RNS, by other physicochemical factors that are also actively involved in the chemical degradation and pathogen inactivation pathways such as UV radiation, high energy electrons, shock waves, and local high temperature. For instance, plasma-induced electrical fields can lead to physical destruction (electroporation or electrostatic destruction) that potentially kills pathogens present in water, and UV radiation is associated with an improved antibacterial efficiency given its capability to destroy bacterial DNA.[12–14] Nonetheless, plasma alone produces relatively low densities of reactive species ($OH^•$, O, H_2O_2) not effectively penetrating the gas–liquid interface to influence the target pathogens and reach a 100% degradation efficiency of organic molecules.[16] To overcome this issue, few researchers have recently implemented a combinatorial strategy that couples NTAPP with various photocatalysts to generate a higher concentration of ROS and RNS in aqueous solutions.[17,18] For instance, Pandiyaraj *et al.* have investigated the degradation of a direct textile effluent dye using NTAPP alone or coupled with Cu-doped CeO_2 nanoparticles (NPs). Results have revealed that the efficiency of total organic carbon (TOC) removal from the direct effluent increased significantly from 7.5% for the plasma process alone to 55.3% by adding the photocatalyst.[19] Zhou *et al.* have studied the eradication of *Escherichia coli* (*E. coli*) in aqueous solutions using an atmospheric pressure microplasma jet array sustained in different working gases, namely He, Air, N_2 and O_2. The presence of the O_2 atmosphere was revealed to inactivate 99.9% of the present *E. coli* within a 4 min treatment time. Nevertheless, in the presence of a TiO_2 photocatalytic film in the plasma reactor, the time required to kill 99.9% of the *E. coli* was reduced to 1 min.[20] TiO_2 is one of the most preeminent photocatalysts that has conquered a prominent position in several industries to use effluent treatment and water decontamination. The non-toxicity, easy availability, photochemical stability, economic viability and biological inertness are some of the factors that led to the supremacy of TiO_2 compared to other photocatalysts. Nonetheless, TiO_2 has associated with the two following main limitations: (1) the rapid recombination of the electron–hole pair, which hampers the generation of various reactive species such as H_2O_2, O_3, $OH^•$, *etc.* during the photodegradation and decontamination processes and (2) the relatively high bandgap restricting the optical response to the UV range. Therefore, doping TiO_2 with metal is commonly adopted to optimize the bandgap and improve the desired processes efficiency. Copper is one of the most suitable dopants for TiO_2, given its pronounced capability to enhance the light gathering capacity and prevent electron–hole recombination.[21–24]

Given the above, the present study aims at enhancing the ROS and RNS production in wastewater for both an improved inactivation of common pathogens and enhanced degradation of organic pollutants. This will be achieved by the synergetic effect of the AOPs of NTAPP and the photocatalytic activity of TiO_2 and Cu-doped TiO_2 materials. Hence, the first part of the study is devoted to synthesize TiO_2 and Cu–TiO_2 NPs, making use of the hydrothermal method, and then characterize them using field emission scanning electron microscopy (FE-SEM) and X-ray diffraction (XRD). The second part of the study reports the inactivation efficiency of the most common Gram-negative (*E. coli*) pathogenic bacteria inoculated in water and the degradation of direct textile wastewater (DTW) by the concurrent NTAPP/photocatalyst process using various operating conditions. The reactive species generated during the inactivation process are determined by optical emission spectroscopy (OES). Moreover, the degradation efficiency of DTW is

evaluated by UV-Vis spectroscopy. The formation of $OH^{\bullet}$, and H_2O_2 in the contaminated water is investigated by several spectroscopic methods.

2. Experimental procedure

2.1. Materials

The chemicals (analytical grade) used to synthesize TiO_2, and Cu–TiO_2 NPs were purchased from MERCK, India, and were utilized as provided without any further purification. The plasma forming gases were obtained from Jayam Spl Gases, Coimbatore, India. *E. coli* was procured from Microbial type culture collection, Chandigarh, India (*E. coli* – MTCC no. 452). The direct textile wastewater was kindly provided by Junior Textile, Tirupur, Tamil Nadu, India.

2.2. Synthesis and characterization of TiO_2 and Cu–TiO_2 NPs

The synthesis of the TiO_2 and Cu/TiO_2 NPs was performed *via* the hydrothermal method using titanium tetraisopropoxide (TTIP) (purity ≥ 97.0%) and copper sulfate pentahydrate (purity ≥ 98.0%). Initially, 20 ml of TTIP was dissolved in 50 ml of ethanol (purity 99.9%) with a constant stirring for one hour. Subsequently, 2% of diluted hydrochloric acid (HCl, 37%) was added to the precursor solution to maintain the pH at 4.5. 4.98 g of copper sulfate was dissolved in 20 ml of ethanol, then added dropwise into the TiO_2 precursor solution with vigorous stirring to prepare Cu-doped TiO_2. Finally, the obtained solutions were transferred into the separate Teflon-lined autoclave and were heated to around 120 °C for 24 h. After that, they were allowed to cool naturally at room temperature. The precipitates were then taken out carefully and washed with ethanol several times, filtered, and dried in a hot air oven at 60 °C. Subsequently, the obtained product was calcinated at 600 °C for 3 h.[22,23] The acquired TiO_2 and Cu–TiO_2 NPs were used as a photocatalyst to deactivate microorganisms and treat DTW.

The morphology and elemental composition of TiO_2 and Cu–TiO_2 NPs were examined *via* FE-SEM equipped with energy-dispersive X-ray spectroscopy (EDX) (ZEISS SIGMA FESEM, Germany). The phase and structure of the NPs were investigated by a powder XRD (X'pert PRO X-ray Diffractometer, PANalytical, Netherlands) using Cu Kα (λ = 0.154 nm). The photoluminescence and optical properties of the NPs were examined and the corresponding experimental section can be found in the ESI.†

2.3. NTAPP plasma reactor

The NTAPP reactor used for the inactivation of microorganisms and degradation of organic compounds is shown in Fig. 1. A detailed description of the setup and experimental procedure is explained elsewhere.[24] In brief, the reactor has two major components, namely the plasma torch and the AC high voltage (40 kV) and high frequency (50 kHz) power supply. The torch consists of a ring-shaped ground electrode and a rod-shaped live electrode; both made up of copper. The rod-type live electrode is covered by quartz acting as a dielectric to prevent arc transition and is further surrounded by a quartz tube with inner and outer diameters of 11 mm and 15 mm respectively. The ring electrode is positioned underneath the live electrode at a distance of 2.5 cm. The torch is equipped with a separate provision for gas inlet and flow rate is regulated by a mass flow controller (GFC37, AALBORG, USA). The torch assembly is further covered with a Teflon enclosure to avoid electric induction during the treatment.

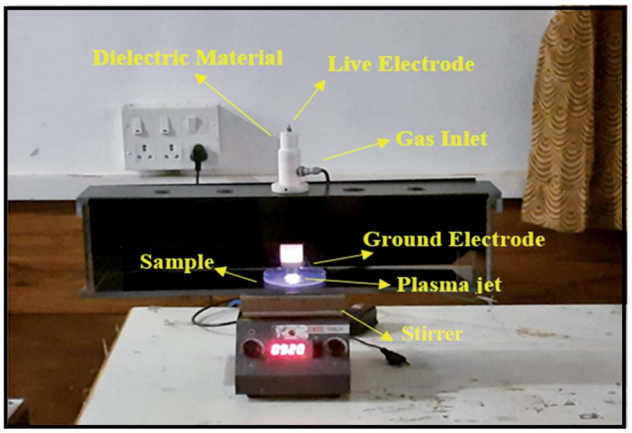

Fig. 1 Plasma jet during the treatment processes.

Moreover, the reactor is equipped with an optical emission spectrometer (HR4000CG UV-NIR, 1 nm, Ocean Optics, Netherlands) to identify the reactive excited species formed in plasma during the inactivation and degradation processes. The emission spectra were recorded in the wavelength region of 200–1100 nm and were analyzed using the Oceanview spectroscopy software. An optical fiber cable (QP400-2-SR-BX) was used to collect the optical signals produced during the process.

2.4. Preparation of the bacterial suspension and plasma treatment

Firstly, 1.9 g of nutrient broth and 5.2 g of nutrient agar were dissolved in 150 ml of deionized water in a separate conical flask. The broth and agar solution were sterilized for 15 min at 121 °C with 151 lbs pressure and cooled at room temperature. After the sterilization process, 20 ml of nutrient agar solution was poured evenly into a separate Petri dish and allowed to solidify. The colonies of *E. coli* were inoculated into a nutrient broth medium and were allowed to mix homogeneously using an orbital shaker for one hour.[25] Thereafter, 20 ml of bacterial suspension broth solution was poured into a Petri plate and brought beneath the plasma torch's orifice. The distance between the surface of the broth solution and the plasma torch orifice was kept constant at 3 mm. After initial arrangements, the plasma forming Ar gas was allowed into the plasma torch through the gas inlet with a constant flow rate of 9 lpm. Subsequently, a high voltage was applied between the two electrodes and adjusted until a stable plasma exited *via* the orifice of the torch. Finally, the Ar plasma jet plume was allowed to strike and treat the bacterial broth solution for different plasma exposure times (0–60 s) with a fixed applied potential of 24 kV.

Table 1 Plasma operating parameters

Applied potential	24 kV
Treatment time	0–60 s
Distance between the live and the ground electrodes	2.5 cm
Distance between the plasma torch and the water surface	3 mm
Plasma-forming gas and gas mixtures	Ar, Ar + N_2 and Ar + O_2
Ar flow rate	9 lpm
Ar + N_2 flow rate	7 lpm + 2 lpm
Ar + O_2 flow rate	7 lpm + 2 lpm

Similarly, the bacterial inactivation process was carried out using 2 different working gas mixtures: Ar + N_2 (7 lpm + 2 lpm) and Ar + O_2 (7 lpm + 2 lpm). After that, the inactivation process was also carried out by combining Ar plasma with the photocatalytic activity of the synthesized NPs (TiO_2 and Cu–TiO_2). In this synergetic treatment process, 20 mg of TiO_2 or Cu–TiO_2 NPs was homogeneously distributed in the *E. coli* bacteria inoculated aqueous solutions, and the resulting solution was treated with Ar plasma using the parameters mentioned above.

After treatment, 100 μl of the treated solution was spread evenly in Petri dishes containing the solidified agar nutrient medium using an L-shaped rod. All Petri dishes were placed in an incubator for 24 h at 37 °C. The survival rate of bacteria was further assessed by the colony counting method.[25] Table 1 describes the typical operating parameters used in the inactivation processes. After bacterial eradication processes, the influence of plasma alone and the synergetic plasma/NPs treatment was further examined on the degradation of direct textile effluent. The same treatment procedure used for the bacterial eradication processes was followed. The treatment time, applied voltage, and distance between the orifice of the plasma jet and the DTW surface were kept constant at 20 min, 24 kV and 3 mm. After plasma treatment, the aqueous solution was filtered using a filter paper (Whatman 40 filter). Finally, the treated and untreated effluent solutions were analyzed by different analytical methods.

2.5. Evaluation of the untreated and plasma-treated aqueous solutions

2.5.1. Determination of ROS. A chemical dosimetry method was employed to identify the presence of $OH^{\bullet}$ radicals in plasma-treated aqueous solutions using terephthalic acid (TA) (C_6H_4-1,4-$(CO_2H)_2$ – purity = 98%). The detailed description of the $OH^{\bullet}$ measurements is described elsewhere.[25–27] TA reacts only with $OH^{\bullet}$ radicals leading to the production of hydroxyterephthalic acid (HTA). The presence of $OH^{\bullet}$ radicals in the plasma-treated aqueous solution was measured by UV light (wavelength: 310 nm) given the fact that the produced HTA molecules emit a fluorescence line at 425 nm as was observed by spectrophotometric measurements (Ocean Optics HR4000CG UV-NIR spectrometer). The intensity of the fluorescent emission was thus related to the increase in HTA concentration directly correlated with that of the trapped $OH^{\bullet}$ radicals by TA. Similarly, the quantification of H_2O_2 in the plasma-treated aqueous solutions was investigated by a spectroscopic technique using potassium titanium(IV) oxalate ($K_2TiO(C_2O_4)\cdot 2H_2O$ – purity = 99% – Sigma Aldrich, India). In order to obtain PTO solution, mixing of PTO (3.54 g), concentrated H_2SO_4 (27.2 ml) and DI water (30 ml) respectively. The volume of the solution was further increased to 100 ml by the addition of the required DI water. After that, 5 ml of the plasma-treated aqueous solution was added to 5 ml of the PTO reagent and was then treated by plasma using the above-used treatment conditions. The resulting color of the aqueous solution was changed into golden-yellow color if plasma-induced H_2O_2 species present in the plasma-treated aqueous solution. Lastly, the absorbance spectra of the aqueous solution were acquired using the spectrophotometer at a wavelength of 400 nm. The concentration of H_2O_2 was obtained based on the following expression:[28]

$$[H_2O_2] = \frac{(A_{pt} - A_{balnk})}{37.4xl} \quad (1)$$

where A_{pt} and A_{blank} are the absorbance of the solution after the plasma treatment and the blank, respectively and l and x the pathlength (cm) of the cuvette and volume (ml) of the solution, respectively.

The presence of ozone in the plasma-treated solutions was further evaluated using the indigo method.[29] Before quantifying O_3 in the solution, an indigo stock solution was prepared by adding 770 mg of potassium indigo trisulfonate into a mixed solution containing 1.0 ml of conc. phosphoric acid and 500 ml of distilled water. After that, 7 ml of conc. H_2SO_4, 10 ml of the obtained indigo solution and 10 g of sodium dihydrogen phosphate were mixed thoroughly in 1000 ml volumetric flask. The mixed solution was then diluted up to the mark resulting in the formation of blue colored indigo reagent solution. Finally, the quantification of the ozone in the aqueous solution was done based on the color-changing spectroscopic method of the obtained indigo reagent solution. In this process, untreated and plasma-treated aqueous solutions were added to 10 ml of indigo reagent solution. If O_3 is present in the solution, the colored reagent will be decolorized, and the absorbance of the decolorized sample was measured at 600 nm using a spectrophotometer. The concentration of ozone was calculated as follows:[29]

$$\text{Ozone concentration in mg } L^{-1} = \frac{\Delta A \times 100}{F \times b \times V} \quad (2)$$

where ΔA, b and V are the difference in absorbance between the sample and the blank, pathlength (cm) and volume of the sample (ml) respectively and $F = 0.42$.

2.6. Assessment of the degradation, pH and electrical conductivity

The percentage of degradation of the DTW with respect to various plasma treatments was monitored *via* a UV-Vis spectrophotometer (Ocean Optics HR4000CG UV-NIR spectrometer) equipped with a Deuterium halogen light source using the following formula:[30]

$$\text{Degradation } (\%) = \frac{A_0 - A_t}{A_0} \times 100 \quad (3)$$

where A_0 and A_t are the initial and final absorbances of the aqueous solution respectively.

The electrical conductivity (EC) and pH of the plasma-treated water were measured using a digital EC meter-611 (Elico Ltd, India) and a digital pH meter (pHep, HANNA Instruments, USA) respectively.

3. Result and discussion

3.1. Morphology of TiO_2 and Cu–TiO_2 NPs

SEM images revealed that TiO_2 NPs exhibited a flower-like structure, presenting groups of well-aligned nanorods having diameter of 30 nm (Fig. 2a). This flower-like TiO_2 morphology was previously reported to trigger a significant photocatalytic performance owing to its large contact areas.[31] The morphology of the Cu–TiO_2 NPs exhibited a tripod/multipod-like structure with more or less a uniform size of each pod (approximately 300 nm in length) (Fig. 2b). This observation confirms that the Cu doping significantly affected the morphology of the TiO_2 NPs as was also observed previously.[31,32]

3.2. Crystal structure of TiO_2 and Cu–TiO_2 NPs – XRD analysis

XRD analysis was performed to investigate the phase composition of the synthesized TiO_2 and Cu–TiO_2 NPs. Fig. 3a depicts the XRD pattern of the TiO_2 NPs that revealed various strong diffraction peaks at 2θ values of 25.70° (101), 38.05° (004), 48.11° (200), 54.81° (105), 62.67° (204), 69.76° (116) and 75.1° (215) matching well with the TiO_2 anatase phase (JCPDS 21-1272) that is considered to be the most photoactive phase.[22] Fig. 3b displays the XRD pattern of the Cu–TiO_2 NPs that exhibited similar peaks of TiO_2. Nonetheless, no peaks due to Cu (CuO and Cu_2O) were observed in the XRD pattern attributed to the incorporation of Cu into the TiO_2 *via* replacing Ti. The absence of such peaks is presumably because the ionic radii of Cu^{2+} (0.73 pm) are very similar to the ionic radii of Ti^{4+} (0.68 pm).[33,34] Nevertheless, the EDX spectrum confirmed the incorporation of Cu into TiO_2 NPs (Fig. 4). Finally, the average crystallite size of TiO_2 and Cu–TiO_2 NPs were found to be 6.89 and 6.01 nm, respectively, as estimated by Debye–Scherrer's equation. Ultraviolet-visible diffuse reflection spectroscopy (UV-Vis DRS) and photoluminescence emission spectral analyses can be found in the ESI.†

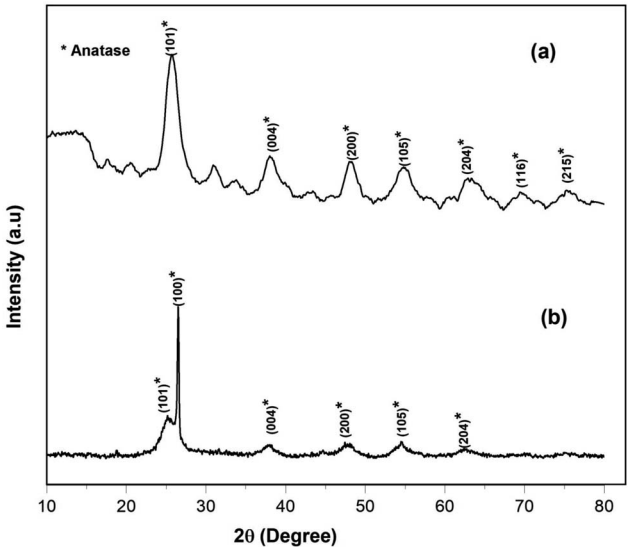

Fig. 3 XRD patterns of the synthesized (a) TiO_2 and (b) Cu–TiO_2 NPs.

3.3. Identification of excited species: *in situ* OES analysis in the presence of *E. coli* suspensions

The generation of excited species in plasma during the inactivation of *E. coli* under various treatment conditions was examined by OES as depicted in Fig. 5.

The OES spectrum of the Ar plasma jet alone exhibited various major peaks due to excited Ar species (690–900 nm), $OH^{\bullet}$ (309 nm) and N_2 second positive system (NSPS) (334 and 354 nm) (Fig. 5a). The presence of hydroxyl ($OH^{\bullet}$) radicals and NSPS may be due to the interaction of plasma species with moisture and species present in the surrounding atmosphere. The OES spectrum of the Ar plasma jet during the inactivation of *E. coli* also displayed similar emission lines. Furthermore,

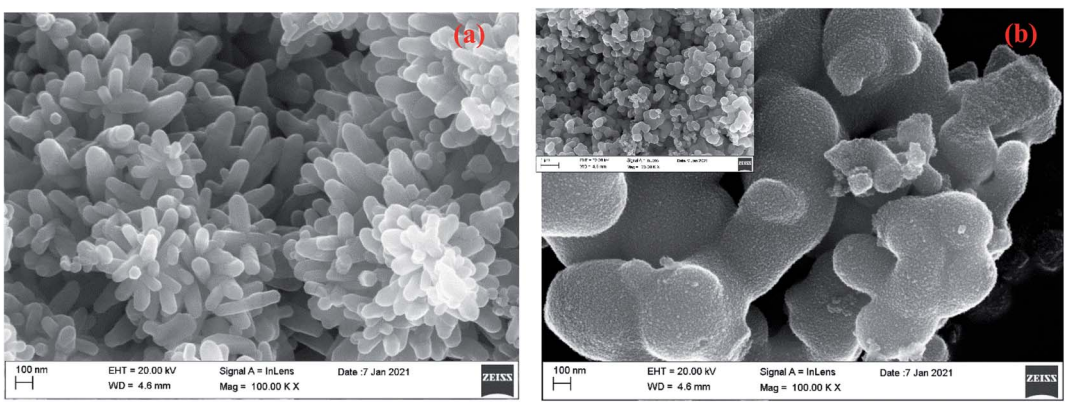

Fig. 2 FESEM images of the synthesized (a) TiO_2 and (b) Cu–TiO_2 NPs.

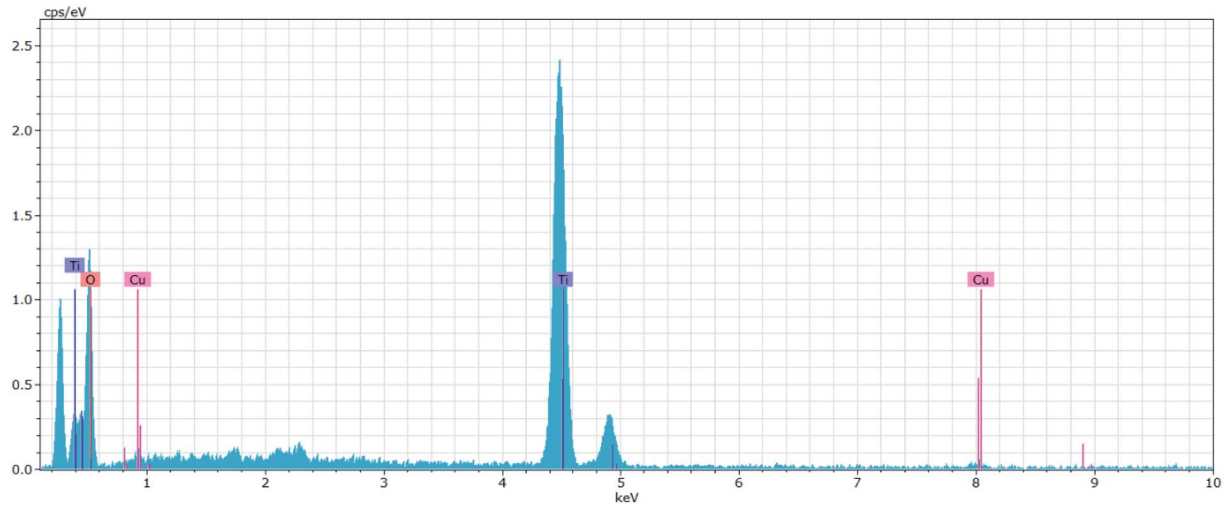

Fig. 4 EDX spectrum of the Cu–TiO_2 NPs.

two new spectral lines were observed at 771 and 842 nm due to the formation of atomic oxygen species attributed to the interaction of high energy electrons in plasma with O_2 molecules ($e^- + O_2 \rightarrow O + O$) and the fragmentation of H_2O molecules in the aqueous solution.[24,25] The OES spectra of the Ar + N_2 and Ar + O_2 plasmas presented the same emission lines attributed to $OH^\bullet$, O, NSPS and Ar species. However, the intensity of the Ar emission lines was found to decrease substantially due to interaction of Ar species with N_2 and O_2 in plasma and with water molecules in the aqueous environment. These interactions triggered the increase in the intensity of the emission lines due to O, $OH^\bullet$ and N_2 species ($Ar^* + H_2O \rightarrow Ar + OH^\bullet + H$; $Ar^* + N_2 \rightarrow Ar + N_2^*$; $N_2^* + H_2O \rightarrow N_2 + OH^\bullet + H$) (Fig. 5b).[35–39] The observed reactive species were associated with an enhanced pathogen inactivation efficacy during the treatment. Fig. 5c portrays the OES spectra of the Ar plasma jet striking the *E. coli* suspension in the presence of TiO_2 and Cu–TiO_2 NPs. The spectrum corresponding to the presence of TiO_2 NPs exhibited new spectral lines at 540–570 nm due to TiO.[35] Finally, when Ar plasma deactivation processes were coupled with Cu–TiO_2 NPs, the OES spectrum showed various additional spectral lines due to Cu^{2+} and Cu^+ (356, 376, 415, 518, 588, 603 and 612 nm).[40]

Consequently, the intensity of the spectral lines due to Ti, O, $OH^\bullet$ and NSPS were observed to increase compared to the other treatment conditions. The generation of Cu species (Cu^{2+} and Cu^+) may be attributed to the redox reaction of Cu ions when they interact with plasma species during the inactivation processes ($Cu^+ + O \leftrightarrow Cu^{2+} + e^-$).[41] The obtained Cu^{2+} and Cu^+ presumably contributed to the increase in ROS concentration during the processes by preventing the recombination of the photo-generated electron–hole pairs that capture the energetic electrons during the interaction of UV-photons in plasma with TiO_2 ($TiO_2 + h\nu \rightarrow e^- + h^+$).[38,39] This prolonged lifetime of the holes in the valence bands probably led to further interaction between those photo-generated holes and water molecules, which ultimately resulted in more hydroxyl radicals ($h^+ + H_2O \rightarrow OH^\bullet + H^+$).[39,40] Subsequently, the photo-generated electrons interacted with oxygen molecules producing superoxide ions. Besides the catalytic reactions, the energetic plasma species also contributed to the generation of various ROS and RNS during the inactivation processes *via* their reaction with the liquid and gas phases as presented in the following reactions.[24,42–45]

$$Ar^* + H_2O \rightarrow Ar + OH^\bullet + H \quad (R1)$$

$$e^- + H_2O \rightarrow H^+ + OH^\bullet + 2e^- \quad (R2)$$

$$O_2 + e^- \rightarrow O + O \quad (R3)$$

$$Ar^* + N_2 \rightarrow Ar + N_2^* \quad (R4)$$

$$N_2^* + H_2O_{(g)} \rightarrow N_2 + O_{(g)} + H \quad (R5)$$

Owing to the above-stated facts, the intensity of the emission lines corresponding to ROS significantly increased when plasma treatment was combined with Cu–TiO_2 NPs. Overall, the OES results indicated the enhanced capacity of the combinatorial strategy involving Ar plasma and Cu–TiO_2 NPs in generating significantly higher concentrations of ROS and RNS than other treatment conditions, which are expected to improve the bacteria deactivation efficiency and degradation of toxic organic pollutants.

3.4. Assessment of $OH^\bullet$, H_2O_2, and O_3 generation in the treated solutions

The inactivation of the targeted pathogens in the aqueous solution is mainly due, amongst other factors, to the generation of $OH^\bullet$ and H_2O_2 given their pronounced oxidation potential. Thus, it is important to investigate the presence of $OH^\bullet$ and H_2O_2 in aqueous media during the different plasma inactivation processes. This *in situ* generation of hydroxyl radicals was initially determined by a chemical dosimetry method. Fig. 6 depicts the variation in the fluorescence emission intensity of HTA solution upon the various treatment conditions. Results

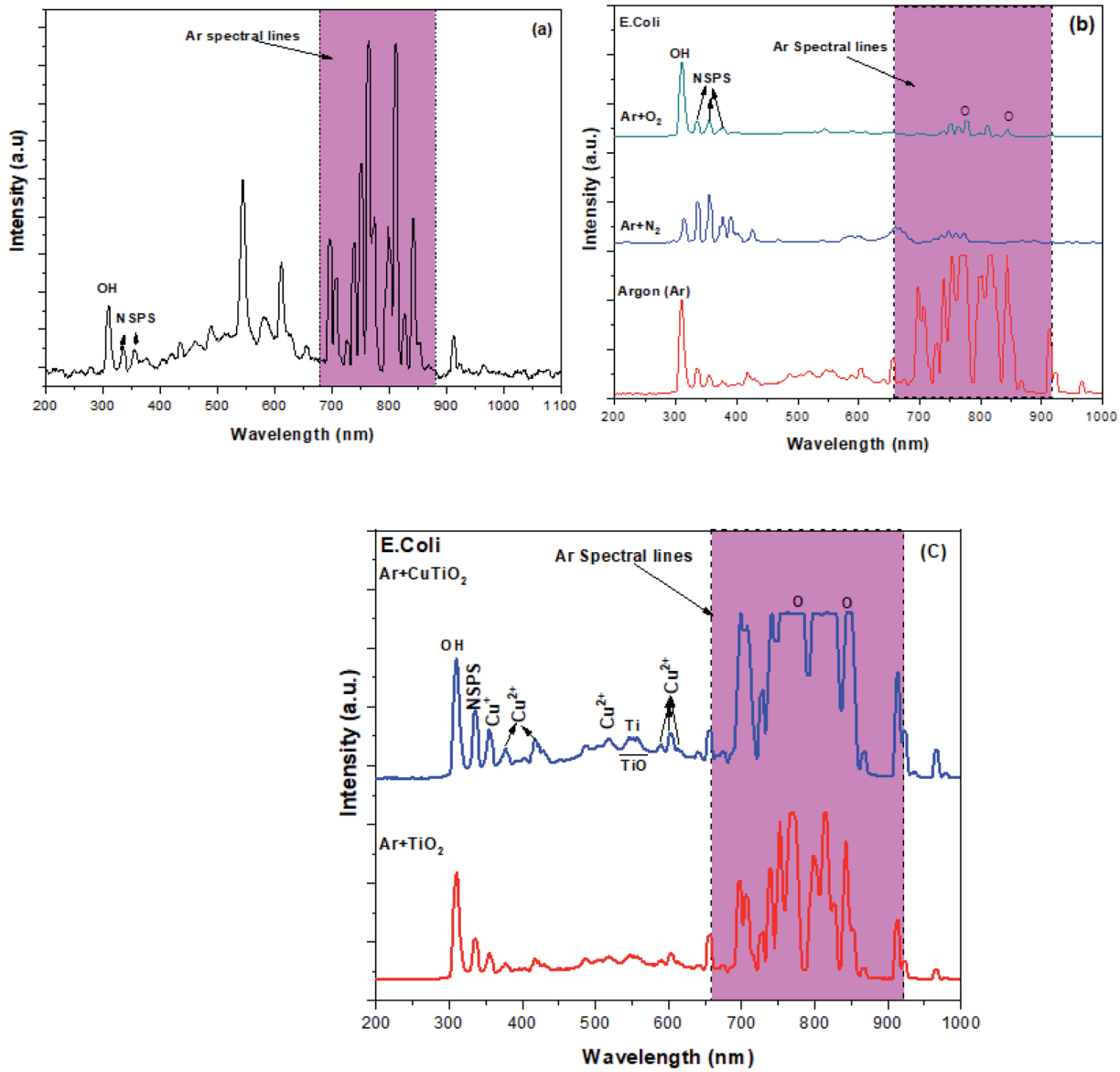

Fig. 5 OES spectra of the plasma jet in the absence and presence of the target bacterial suspension with or without photocatalytic NPs (a) Ar plasma alone, (b) Ar plasma, Ar + N_2 plasma and Ar + O_2 plasma during *E. coli* inactivation and (c) Ar plasma combined with TiO_2 and Cu–TiO_2 NPs during *E. coli* inactivation.

showed that the fluorescence emission intensity of Ar plasma-treated HTA solution (574.2 a.u.) markedly increased when reactive gases were admixed to Ar and when NPs were added to the solution in the following ascending order: Ar + N_2 plasma < Ar + O_2 plasma < Ar plasma + TiO_2 NPs < Ar plasma + Cu–TiO_2 NPs. The results confirmed that Ar plasma treatment combined with Cu–TiO_2 NPs triggered the formation of the highest concentration of hydroxyl radicals in the aqueous solution as revealed by the obtained maximal absorbance intensity (934.4 a.u.) for this treatment condition.

Similarly, the concentration of H_2O_2 in the different aqueous solutions was determined by a spectroscopic method using potassium titanium(IV) oxalate. The variation in the concentration of H_2O_2 followed the same trends as that of the $OH^{\bullet}$ measurements (Fig. 6). Results also highlighted the fact that the formation of H_2O_2 in the aqueous medium depends on the generation of $OH^{\bullet}$ that recombines to form H_2O_2 ($OH^{\bullet} + OH^{\bullet} \rightarrow H_2O_2$).[44,45] Once again, results confirmed that the combination of plasma treatment with Cu–TiO_2 photocatalysts produced a higher concentration of reactive species which is believed to facilitate the deactivation of various pathogens present in the aqueous solution.

Fig. 7a presents the absorbance spectra of the indigo reagent mixed with various solutions subjected to the different treatment conditions. The untreated aqueous solution exhibited a strong absorbance peak at 600 nm with a maximal absorbance intensity of 1.5 a.u. The intensity of the absorbance peaks was found to decrease in the following descending order: untreated > Ar plasma > Ar + N_2 plasma > Ar plasma + TiO_2 NPs > Ar plasma + Cu–TiO_2 NPs > Ar + O_2 plasma. The formation of the

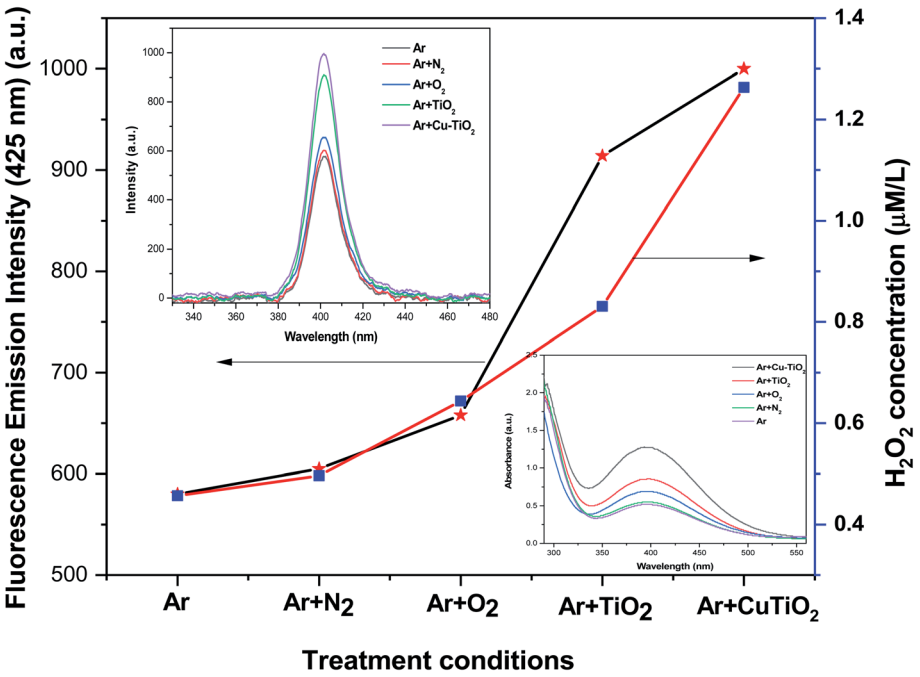

Fig. 6 Variation in the concentration of H_2O_2 and $OH^{\bullet}$ with respect to the treatment condition.

highest concentration of ozone in the Ar + O_2 plasma case confirmed by the quantification of ozone using eqn (2) may be attributed to the following reaction: $O_2 + O \rightarrow O_3$ (Fig. 7b). In addition, the obtained ozone presumably interacted with electrons producing ozonide ions (O_3^-) that in turn generated more $OH^{\bullet}$ radicals, as presented in the following reactions[46,47]

$$O_3 + e^- \rightarrow O_3^{-\bullet} \quad (R6)$$

$$O_3^{-\bullet} + 2H^+ \rightarrow H_2O_2 + O \quad (R7)$$

$$H_2O_2 + e^- \rightarrow 2OH^{\bullet} \quad (R8)$$

3.5. Inactivation/killing processes of *E. coli*

The influence of the different treatment conditions on the inactivation/killing of *E. coli* was examined by the colony-forming unit (CFU) method as portrayed in Fig. 8. It shows the photographs of *E. coli* plated on agar after subjecting the inoculated suspensions to the different treatment conditions and the corresponding quantitative measurements of the CFUs. A greater number of colonies (350 CFU ml^{-1}) was detected in the case of the control sample compared to all other treated samples. After 15 s of Ar plasma treatment, the number of colonies slightly decreased and continued to decrease with increasing the treatment time progressively. Finally, only 30 CFUs were observed for a plasma exposure time of 60 s, which

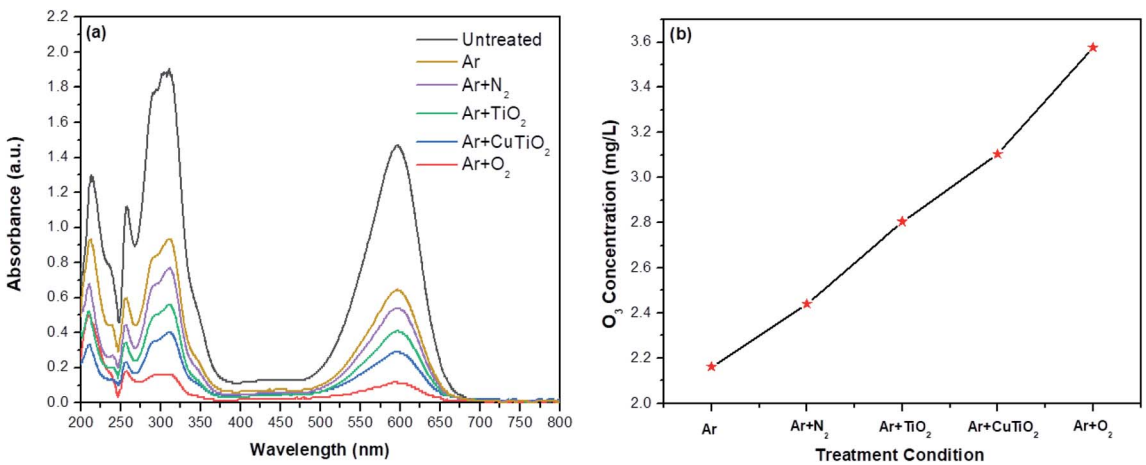

Fig. 7 Estimation of O_3 concentration in solutions subjected to different treatment conditions. (a) Absorbance spectra of the indigo reaction and (b) O_3 concentration.

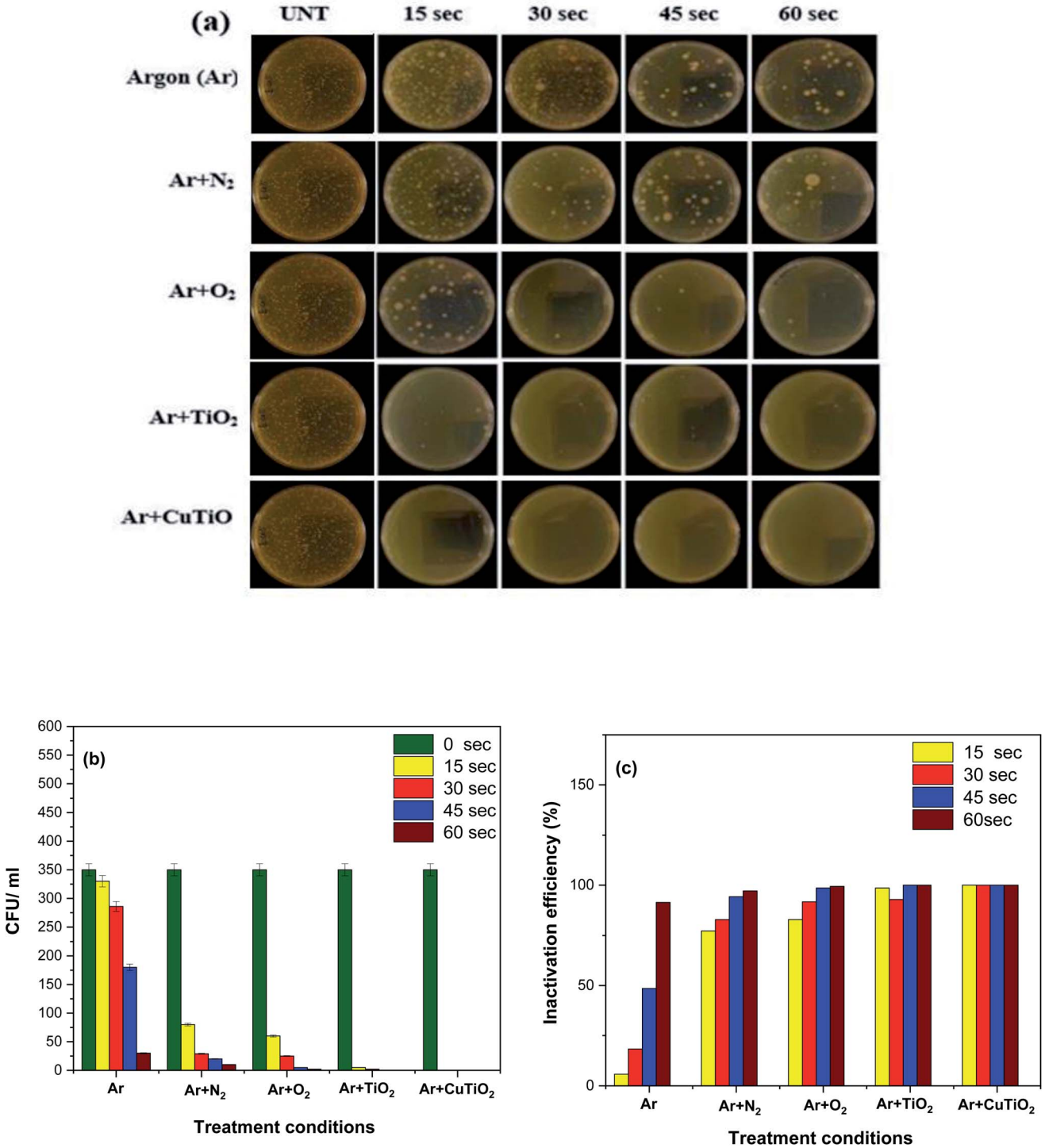

Fig. 8 Inactivation/killing of *E. coli*. (a) Growth of *E. coli* on agar after subjecting the suspension to different treatment conditions and exposure times; (b) CFU count as a function of the treatment condition and (c) *E. coli* inactivation efficiency as a function of the treatment.

corresponds to an inactivation efficiency of 97.1% (Fig. 8b and c). This reduction in the number of CFUs was mainly caused by increasing ROS and RNS such as $OH^{\bullet}$, O, H_2O_2 and NO_3^- as the treatment time increased. At early stages, plasma treatment produced a meager amount of reactive species that could not trigger severe damage to the outer membrane of bacteria. Even if the outer membrane were affected by minor damages, *E. coli* bacteria would not be killed or inactivated due to their characteristic effective self-defense and self-healing mechanisms that protect them.[48–51]

In contrast, the generation of higher concentrations of reactive species upon longer plasma exposures caused severe

damages to the cell membrane, which swiftly suppressed the self-protection mechanisms of the *E. coli* bacteria resulting in a higher inactivation/killing rate. The killing/inactivation processes were further examined by treating the bacterial suspensions with Ar + O_2 and Ar + N_2 plasmas for various exposure times. Ar + N_2 plasma treatment significantly decreased the number of colonies to 80 CFU ml^{-1} after a relatively short treatment time of 15 s and led to a complete bacterial eradication upon a treatment time of 60 s. The inactivation/killing rate of *E. coli* was higher when treating the solution with Ar + O_2 compared to Ar + N_2 plasma due to the generation of higher concentrations of ROS and the emission of a more extensive extent of UV radiation during the processes (Fig. 8b and c). When the processes were carried out *via* the combination of the AOPs of Ar plasma with the photocatalytic reactions of TiO_2 and Cu–TiO_2 NPs, the bacterial eradication rate was significantly improved. In particular, the presence of Cu–TiO_2 NPs could lead to a complete inactivation/killing of *E. coli* in the aqueous solution and, as such, a 100% deactivation efficacy within only 15 s of plasma exposure (Fig. 8b and c). The observed improved results obtained when implementing the combinatorial plasma-photocatalysis strategy might be attributed to the generation of higher concentrations of ROS (*e.g.*, H_2O_2, O, O_3, and $OH^{\bullet}$) in the aqueous media resulting from combined plasma-electron impact phenomena and plasma-photocatalysis processes. During the inactivation/killing of bacteria by plasma-photocatalysis reactions, Ar plasma produced UV photons absorbed by TiO_2 NPs, resulting in the generation of electron–hole pairs. The photo-generated holes reacted with water molecules to form $OH^{\bullet}$ radicals. Simultaneously, superoxide ions radical ($O_2^{-\bullet}$) were formed *via* the interaction of photoelectrons with oxygen molecules. The formation of reactive species during the plasma catalytic process is shown in the following reactions[23,37,50,51]

$$TiO_2 + h\nu \rightarrow e^- + h^+ \quad (R9)$$

$$h^+ + H_2O \rightarrow H^{\bullet} + OH^{\bullet} \quad (R10)$$

$$e^- + O_2 \rightarrow O_2^{-\bullet} \quad (R11)$$

$$2O_2^- + 2H^+ \rightarrow H_2O_2 + O_2 \quad (R12)$$

The obtained reactive species constitute one of the main factors killing/inactivating the pathogens in aqueous media. In fact, those species oxidized the lipid peroxide to form hydroperoxide and triggered oxidative stress in the bacterial cells engendering devastating effects on the structure and activity of proteins which ultimately killed the bacteria. Moreover, Zhou *et al.* have reported that the positioning of the bacteria on the surface of TiO_2 photocatalysts affords an additional mechanism for their inactivation.[20] In fact, this contact between TiO_2 and the bacterial cell leads to a direct exchange of an electron–hole on the surface of the cell envelope that leads to formation of ROS. Once crossing the envelope, the ROS will oxidize and damage the intracellular components of the DNA and intracellular proteins, thus killing the cell. Furthermore, the direct

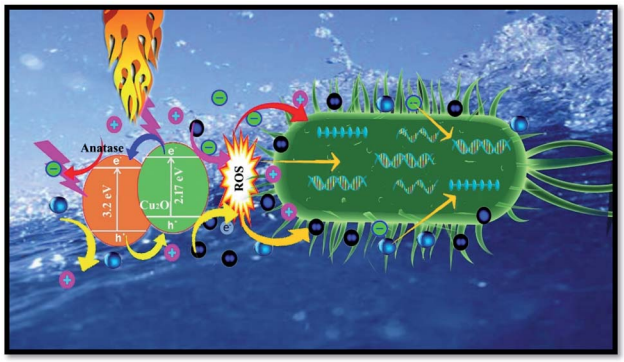

Fig. 9 Schematic diagram of the effects of plasma AOPs and NP photocatalysis reactions on the inactivation/killing of a bacterial cell.

penetration of metal ions through the cell membrane was associated with a rupture of the nucleic acid and protein, resulting in the inactivation or eradication of the bacterial cells. A schematic diagram of the microbial inactivation upon the combined plasma-NPs treatment is shown in Fig. 9. Despite the numerous stated advantages of the combined plasma treatment with TiO_2 catalysis, two major constraints exist. The first one is the fast recombination of the photo-generated electron–hole pairs during the process and the second one resides in the limited optical response within the UV range owing to the wide bandgap.[22] The use of Cu–TiO_2 NPs instead of TiO_2 NPs comes to overcome the limitations in this combinatorial strategy.

In fact, the doping of copper into the TiO_2 plays a significant role in ROS production by capturing photoelectrons that reduce Cu^{2+} oxidation states into Cu^+ ($Cu^{2+} + e^- \rightarrow Cu^+$). In their turn, Cu^+ ions can further re-oxidize by the presence of oxygen and hydrogen peroxide in the solution to form Cu^{2+} ($Cu^+ + O_2 \rightarrow Cu^{2+} + e^-$; $Cu^+ + H_2O_2 \rightarrow Cu^{2+} + 2OH^{\bullet}$). The obtained electrons also interact with oxygen molecules in an aqueous solution to form superoxide (O_2^-) ($e^- + O_2 \rightarrow O_2^-$). Concurrently, the photo-generated holes react with H_2O molecules to generate $OH^{\bullet}$ radicals ($h^+ + H_2O \rightarrow OH^{\bullet} + H^+$). The ionic states of Cu (Cu^{2+} and Cu^+) also contribute to the generation of $OH^{\bullet}$ by reacting with H_2O and H_2O_2 ($Cu^{2+} + H_2O \rightarrow Cu^+ + OH^{\bullet} + H$; $Cu^+ + H_2O_2 \rightarrow Cu^{2+} + 2OH^{\bullet}$).[23,52] Moreover, the doping of Cu can improve the light gathering capacity of TiO_2 *i.e.*, by extending the UV range to the visible range.[22,23] Owing to the obtained evident results and the above-stated facts, one can conclude that the treatment processes carried out by the combination of plasma with Cu/TiO_2 NPs could produce significantly higher concentrations of reactive species than the plasma treatment alone enhanced the killing/inactivation of bacteria.

3.6. pH and conductivity of the untreated and treated solutions

Given the drastic effects of acidic environments on bacteria, the determination of the pH is one of the important validations indicating their successful inactivation/eradication. The pH of untreated and all treated aqueous solutions were measured, and the corresponding results are presented in Fig. 10. The pH

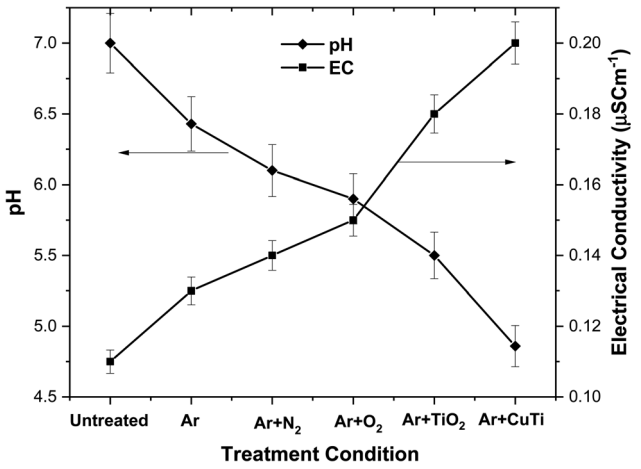

Fig. 10 Variation of the EC and pH as a function of the implemented treatment conditions.

of the untreated aqueous solution was 7.0, thus indicating a neutral medium. After performing the various treatments, the pH of the aqueous medium decreased in the following order: Ar plasma > Ar + N_2 plasma > Ar + O_2 plasma > Ar plasma + TiO_2 NPs > Ar plasma + Cu–TiO_2 NPs. Results confirmed that the natural aquatic medium was converted into acidic media due to the formation of various acidic compounds such nitric and nitrous acids ($N_2 + e^- \rightarrow N^\bullet + N^\bullet$; $N^\bullet + O_2 \rightarrow NO + O^\bullet$; $NO + O_3 \rightarrow NO_2 + O_2$; $NO_2 + OH^\bullet \rightarrow HNO_3 \rightarrow H^+ + NO_3^-$; $NO + OH^\bullet \rightarrow HNO_2 \rightarrow H^+ + NO_2^-$).[42,44,53,54] In an acidic medium, the amino acids and functional groups of microorganisms are severely affected, leading to the denaturation of their proteins which compromises their activity and ultimately triggers their death.[55,56] Fig. 10 also shows the variation in the EC of the aqueous media pre-and post-treatment. Results revealed that the EC of the untreated solution was 0.11 μS cm^{-1} and increased post-treatment in the following order of treatment conditions: Ar plasma < Ar + N_2 plasma < Ar + O_2 plasma < Ar plasma + TiO_2 NPs < Ar plasma + Cu–TiO_2 NPs. This may be ascribed to the formation of various ions in the solution, which can penetrate the cell wall of the microbes and further hamper their normal activity.[57] Given the fact that the presence of TiO_2 and Cu–TiO_2 NPs could give significantly better results compared to plasma alone, all the following investigations will be limited to the treatment conditions involving the combinatorial strategy: Ar plasma + TiO_2 NPs and Ar plasma + Cu–TiO_2 NPs. Ar plasma alone will be also tested for comparison purposes.

3.7. Degradation of DTW

The action of the synergetic treatment was further studied by evaluating the degradation of DTW. Fig. 11a portrays the UV-Vis absorbance spectra of untreated and treated DTW under various conditions. The absorbance spectrum of untreated DTW exhibited a wide absorbance peak in the range of 551–661 nm attributed to the existence of different organic compounds in the DTW. After Ar plasma treatment alone, the intensity of the absorbance peak slightly decreased, corresponding to a degradation percentage of 16.1% (Fig. 11b).

The intensity of the absorbance peak further decreased when Ar plasma was combined with TiO_2 NPs, resulting in a degradation efficiency of 40.3% of the organic molecules in the DTW. Interestingly, the intensity of the absorbance peak significantly dropped when Ar plasma was coupled with Cu–TiO_2 NPs to reach a maximal degradation percentage of 55.7%. The increase in the degradation percentage of organic contaminants in the DTW is most probably attributed to the formation of various ROS (*e.g.*, $OH^\bullet$ and H_2O_2) during the different processes (Table 2). This increase was perceived to adhere to the following ascending order of treatment condition: Ar plasma < Ar plasma + TiO_2 NPs < Ar plasma + Cu–TiO_2 NPs. The degradation of DTW by the various treatment conditions was further validated by measuring the pH and EC as displayed in Table 2. Results revealed that the pH and EC of the untreated DTW were 8.9 and 0.312 μS cm^{-1}, respectively. A significant decrease in the pH values was perceived after performing the various treatments and went along with the following descending order of

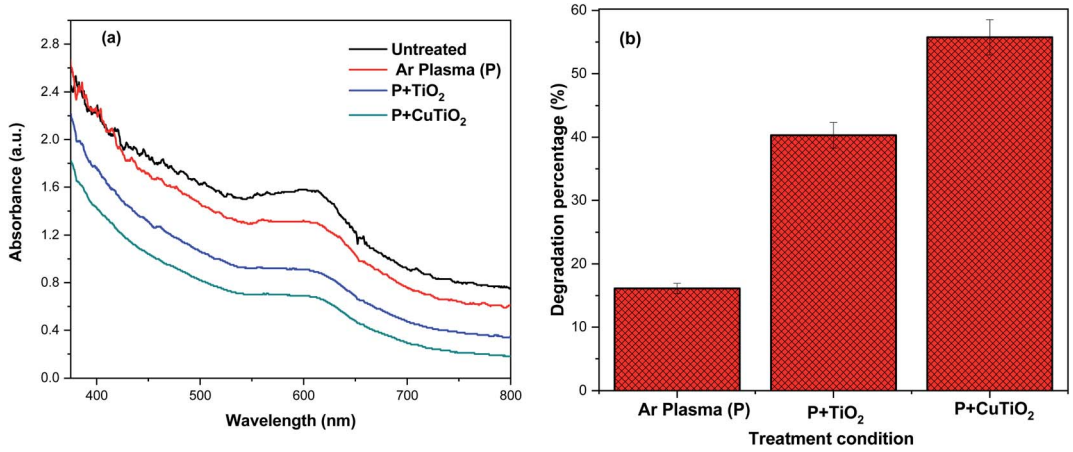

Fig. 11 (a) UV-Vis absorption spectra and (b) degradation percentage of DTW as a function of the treatment condition (Ar plasma alone or coupled with TiO_2 or Cu–TiO_2 NPs).

Table 2 Variation in the fluorescence emission intensity, pH, EC, TOC removal percentage and H_2O_2, between untreated and treated DTW for various operating conditions

Treatment conditions	Fluorescence emission intensity (a.u.)	Concentration of H_2O_2 ($\mu m\ l^{-1}$)	pH	EC ($\mu S\ cm^{-1}$)	% TOC removal
Untreated	—	—	8.9	0.312	—
Ar plasma	1011	0.269	8.1	0.365	16.13
Ar plasma + TiO_2 NPs	2183	1.288	7.5	0.412	40.31
Ar plasma + Cu–TiO_2 NPs	2556	2.137	5.9	0.564	55.76

conditions: untreated > Ar plasma > Ar plasma + TiO_2 NPs > Ar plasma + Cu–TiO_2 NPs. A reverse ascending trend was observed for the EC of the untreated and treated DTW (Table 2). The decrease in the pH of the DTW indicated an increased acidity *via* the formation of various acids (HNO_2 and HNO_3) resulting from the breakdown and oxidation of the present organic molecules. The increase in the EC may be due to the generation of various ionic species in the plasma-treated DTW. Moreover, results showed that a maximum of 55.7% of TOC was removed when the DTW was synergistically subjected to the AOPs of Ar plasma and the photocatalysis processes of Cu–TiO_2 NPs. The above-observed results offered an additional strong validation that the treatment carried out by the combination of Ar plasma with Cu–TiO_2 NPs is more effective in decomposing numerous organic molecules in DTW than the Ar plasma treatment alone owing to the generation of higher concentrations of various ROS and RNS.

4. Conclusion

The research investigated the synergetic effects of the AOPs of an NTAPP treatment and the photocatalytic activity of TiO_2 and Cu–TiO_2 NPs on both the inactivation of bacteria and the degradation of organic pollutants in wastewater. Thus, the first part of the investigation was devoted to synthesize TiO_2 and Cu–TiO_2 NPs by the hydrothermal method. The morphology and phase of the NPs were then studied, making use of FE-SEM and XRD measurements. FE-SEM results revealed that TiO_2 and Cu–TiO_2 NPs exhibited flower-like and multipod-like structures, respectively. XRD analysis indicated a typical anatase structure for both TiO_2 and Cu–TiO_2 NPs. Moreover, the successful incorporation of Cu ions into the TiO_2 lattice was evidently confirmed by EDX upon Cu-doping of the NPs. The NPs bandgap, that was obtained by UV-Vis DRS, decreased when TiO_2 NPs were doped with Cu. Moreover, PL analysis revealed that the emission intensity of the Cu-doped TiO_2 NPs was higher than that of TiO_2 NPs owing to the formation of oxygen vacancies that hinder the recombination rate of electrons which improved the photocatalytic activity performance. The second part of the investigation explored the influence of various treatment conditions (Ar plasma, Ar + N_2 plasma, Ar + O_2 plasma, Ar plasma + TiO_2 NPs and Ar plasma + Cu–TiO_2 NPs) on the inactivation/killing of Gram-negative (*E. coli*) bacteria and degradation of DTW. OES and several other spectroscopic analyses evidently showed that the synergetic treatment implicating Cu–TiO_2 NPs and Ar plasma generated the highest density of ROS (*e.g.* $OH^{\bullet}$ and H_2O_2), which led to an enhanced inactivation efficiency of the pathogens and degradation efficiency of DTW. The results were further corroborated by pH, EC, and TOC removal efficiency measurements. Overall, the present extensive analysis showed that the combinatorial strategy involving the photocatalytic activity of Cu–TiO_2 and oxidation processes of NTAPP has a great potential as a full one-step wastewater treatment concurrently killing microorganisms and degrading toxic organic compounds.

Conflicts of interest

There are no conflicts of interest to declare.

Acknowledgements

Dr K. Navaneetha Pandiyaraj grateful to the Science and Engineering Research Board (SERB) (EMR/2016/006812 Dated: 02-Nov-2017) and Department of Science and Technology – Fund for Improvement of S&T infrastructure in universities & higher educational institutions (DST-FIST) Government of India for the financial support. Dr Rouba Ghobeira would like to thank the Research Foundation Flanders-Belgium (FWO – grant number 12ZC720N) for financing her post-doctoral position. MP would like to thank SNR Sons Charitable Trust and Sri Ramakrishna Engineering College, Coimbatore, India.

References

1 P. Sun, H. Wu, N. Bai, H. Zhou, R. Wang, H. Feng, W. Zhu, J. Zhang and J. Fang, Inactivation of Bacillus subtilis spores in water by a direct-current, cold atmospheric-pressure air plasma microjet, *Plasma Processes Polym.*, 2012, **9**, 157–164.
2 World Health Organization (WHO), *Emerging Issues in Water and Infectious Disease*, World Health Organization (WHO), Geneva, 2003.
3 World Health Organization (WHO), *Guidelines for Drinking-WaterQuality*, World Health Organization (WHO), Geneva, 3rd edn, 2008, vol. 1.
4 J. P. S. Cabral, Water microbiology. Bacterial pathogens and water, *Int. J. Environ. Res. Public Health*, 2010, **7**, 3657–3703.
5 H. He, Z. Luo and C. Yu, Embellish zinc tungstate nanorods with silver chloride nanoparticles for enhanced photocatalytic, antibacterial and antifouling performance, *Colloids Surf., A*, 2021, **613**, 126099–126105.

6 H. He, Z. Luo and C. Yu, Diatomite-anchored g-C3N4 nanosheets for selective removal of organic dyes, *J. Alloys Compd.*, 2020, **816**, 152652–152659.

7 H. He, Z. Luo and C. Yu, Multifunctional $ZnWO_4$ nanoparticles for photocatalytic removal of pollutants and disinfection of bacteria, *J. Photochem. Photobiol., A*, 2020, **401**, 112735–112743.

8 H. He, J. Li, C. Yu and Z. Luo, Surface decoration of microdisk-like g-C_3N_4/diatomite with Ag/AgCl nanoparticles for application in Cr(VI) reduction, *Sustainable Mater. Technol.*, 2019, **22**, e00127.

9 C. H. Deng, J. L. Gong, G. M. Zeng, C. G. Niu, Q. Y. Niu, W. Zhang and H. Y. Liu, Inactivation performance and mechanism of Escherichia coli in aqueous system exposed to iron oxide loaded graphene nanocomposites, *J. Hazard. Mater.*, 2014, **276**, 66–76.

10 S. M. AlShehri, J. Ahmed, T. Ahamad, B. M. Almaswari and A. Khan, Efficient photodegradation of methylthioninium chloride dye in aqueous using barium tungstate nanoparticles, *J. Nanopart. Res.*, 2017, **19**, 289–302.

11 H. He, Z. Luo, Z. Y. Tang and C. Yu, Controllable construction of $ZnWO_4$ nanostructure with enhanced performance for photosensitized Cr(VI) reduction, *Appl. Surf. Sci.*, 2019, **490**, 460–468.

12 L. Q. Wang, Y. Y. Tong, J. M. Feng, J. G. Hou, J. Li, X. G. Hou and J. Liang, G-C3N4-based films: a rising star for photoelectrochemical water splitting, *Sustainable Mater. Technol.*, 2019, **19**, e00089.

13 B. Niu and Z. M. Xu, Innovating e-waste recycling: from waste multi-layer ceramic capacitors to Nb-Pb codoped and ag-Pd-Sn-Ni loaded $BaTiO_3$ nano-photocatalyst through one-step ball milling process, *Sustainable Mater. Technol.*, 2019, **21**, e00101.

14 E. S. M. Mouelead, J. O. Tijani, K. O. Badmus, O. Pereao, O. Babajide, O. O. Fatoba, C. Zhang, T. Shao, E. Sosnin, V. Tarasenko, K. Laatikainen and L. F. Petrika, A critical review on ozone and co-species, generation and reaction mechanisms in plasma induced by dielectric barrier discharge technologies for wastewater remediation, *J. Environ. Chem. Eng.*, 2021, **9**, 105758.

15 S. M. AlShehri, J. Ahmed, T. Ahamada, P. Arunachalama, T. Ahmad and A. Khan, Bifunctional electro-catalytic performances of $CoWO_4$ nanocubes for water redox reactions (OER/ORR), *RSC Adv.*, 2017, **7**, 45615–45623.

16 X. Zhang, R. Zhou, K. Bazaka, Y. Liu, R. Zhou, G. Chen, Z. Chen, Q. Liu, S. Yang and K. Ostrikov, Quantification of plasma produced OH radical density for water sterilization, *Plasma Processes Polym.*, 2018, **15**, 1700241.

17 H. Guo, N. Jiang, H. Wang, K. Shang, N. Lu, J. Li and Y. Wu, Enhanced catalytic performance of graphene-TiO_2 nanocomposites for synergetic degradation of fluoroquinolone antibiotic in pulsed discharge plasma system, *Appl. Catal., B*, 2019, **248**, 552–566.

18 R. Zhou, R. Zhou, D. Alam, T. Zhang, W. Li, Y. Xia, A. Mai-Prochnow, H. An, E. C. Lovell, H. Masood and R. Amal, Plasmacatalytic bubbles using CeO_2 for organic pollutant degradation, *Chem. Eng. J.*, 2021, **403**, 126413.

19 K. Navaneetha Pandiyaraj, D. Vasu, M. C. Ramkumar, R. R. Deshmukh and R. Ghobeira, Improved degradation of textile effluents *via* the synergetic effects of Cu-CeO_2 catalysis and non-thermal atmospheric pressure plasma treatment, *Sep. Purif. Technol.*, 2021, **2**, 118037.

20 R. Zhou, R. Zhou, X. Zhang, J. Li, X. Wang, Q. Chen, S. Yang, Z. Chen, K. Bazaka and K. K. Ostrikov, Synergistic effect of atmospheric-pressure plasma and TiO_2 photocatalysis on inactivation of Escherichia coli cells in aqueous media, *Sci. Rep.*, 2016, **6**, 39552.

21 E. Vassallo, M. Pedroni, T. Silvetti, S. Morandi and M. Brasca, Inactivation of Staphylococcus aureus by the synergistic action of charged and reactive plasma particles, *Plasma Sci. Technol.*, 2020, **22**, 85504.

22 M. Janczarek and E. Kowalska, On the origin of enhanced photocatalytic activity of copper modified titania in the oxidative reaction systems, *Catalysts*, 2017, **7**, 317.

23 K. N. Pandiyaraj, D. Vasu, R. Ghobeira, P. S. E. Tabaei, N. De Geyter, R. Morent, M. Pichumani, P. V. A. Padmanabhanan and R. R. Deshmukh, Dye wastewater degradation by the synergetic effect of an atmospheric pressure plasma treatment and the photocatalytic activity of plasma-functionalized Cu–TiO_2 nanoparticles, *J. Hazard. Mater.*, 2020, 124264.

24 K. Navaneetha Pandiyaraj, D. Vasu, P. V. A. Padmanabhan, M. Pichumani, R. R. Deshmukh and V. Kandavelu, Evaluation of influence of cold atmospheric pressure argon plasma operating parameters on degradation of aqueous solution of Reactive Blue 198 (RB-198), *Plasma Sci. Technol.*, 2020, **22**, 055504.

25 D. Vasu, K. N. Pandiyaraj, P. V. A. Padmanabhan, M. Pichumani, R. R. Deshmukh and S. K. Jaganathan, Degradation of simulated Direct Orange-S (DO-S) textile effluent using nonthermal atmospheric pressure plasma jet, *Environ. Geochem. Health*, 2019, 1–14.

26 P. Jamroz, A. Dzimitrowicz and P. Pohl, Decolorization of organic dyes solution by atmospheric pressure glow discharge system working in a liquid flow-through mode, *Plasma Processes Polym.*, 2018, **15**, 1–7.

27 S. E. Page, W. A. Arnold and K. McNeill, Terephthalate as a probe for photochemically generated hydroxyl radical, *J. Environ. Monit.*, 2010, **12**, 1658–1665.

28 R. M. Sellers, Spectrophotometric determination of hydrogen peroxide using potassium titanium (IV) oxalate, *Analyst*, 1980, **105**, 950–954.

29 L. S. Clesceri, A. E. Greenberg and A. D. Eaton, *Standard methods for the examination of water and wastewater*, American Public Health Association, New York, 1998.

30 P. M. K. Reddy, S. Mahammadunnisa and C. Subrahmanyam, Catalytic non-thermal plasma reactor for mineralization of endosulfan in aqueous medium: A green approach for the treatment of pesticide contaminated water, *Chem. Eng. J.*, 2014, **238**, 157–163.

31 S. S. Mali, H. Kim, C. S. Shim, P. S. Patil, J. H. Kim and C. K. Hong, Surfactant free most probable TiO_2 nanostructures *via* hydrothermal and its dye sensitized solar cell properties, *Sci. Rep.*, 2013, **3**, 1–8.

32 S. Pavasupree, K. Onoda, S. Yoshikawa, A. Simpraditpan and W. Pecharapa, Characterization of flower-like titanate and titania nanowires on titanium plate substrate, *Energy Procedia*, 2013, **34**, 555–562.
33 E. Peter Etape, L. John Ngolui, J. Foba-Tendo, D. M. Yufanyi and B. Victorine Namondo, Synthesis and Characterization of CuO, TiO_2, and CuO-TiO_2 Mixed Oxide by a Modified Oxalate Route, *J. Appl. Chem.*, 2017, **2017**, 1–10.
34 R. Nankya and K. N. Kim, Sol-gel synthesis and characterization of Cu-TiO_2 nanoparticles with enhanced optical and photocatalytic properties, *J. Nanosci. Nanotechnol.*, 2016, **16**, 11631–11634.
35 M. Kakati, B. Bora, U. P. Deshpande, D. M. Phase, V. Sathe, N. P. Lalla, T. Shripathi, S. Sarma, N. K. Joshi and A. K. Das, Study of a supersonic thermal plasma expansion process for synthesis of nanostructured TiO_2, *Thin Solid Films*, 2009, **518**, 84–90.
36 M. C. García, M. Mora, D. Esquivel, J. E. Foster, A. Rodero, C. Jiménez-Sanchidrián and F. J. Romero-Salguero, Microwave atmospheric pressure plasma jets for wastewater treatment: degradation of methylene blue as a model dye, *Chemosphere*, 2017, **180**, 239–246.
37 K. Navaneetha Pandiyaraj, D. Vasu, P. V. A. Padmanabhan, R. Ghobeira, P. S. E. Tabaei, P. Cools, N. De Geyter, R. Morent, R. R. Deshmukh and M. Pichumani, Synergetic effect of the catalytic action of plasma jet deposited TiOx coatings and atmospheric pressure plasma treatment on the degradation of RYRR, *Surf. Coat. Technol.*, 2020, **389**, 125642.
38 R. Zhou, R. Zhou, X. Zhang, J. Li, X. Wang, Q. Chen and K. K. Ostrikov, Synergistic effect of atmospheric-pressure plasma and TiO_2 photocatalysis on inactivation of Escherichia coli cells in aqueous media, *Sci. Rep.*, 2016, **6**, 39552.
39 S. Mathew, P. Ganguly, S. Rhatigan, V. Kumaravel, C. Byrne, S. J. Hinder, J. Bartlett, M. Nolan and S. C. Pillai, Cu-Doped TiO_2: Visible Light Assisted Photocatalytic Antimicrobial Activity, *Appl. Sci.*, 2018, **8**, 2067.
40 B. Yotsombat, S. Davydov, P. Poolcharuansin, T. Vilaithong and I. G. Brown, Optical emission spectra of a copper plasma produced by a metal vapour vacuum arc plasma source, *J. Phys. D: Appl. Phys.*, 2001, **34**, 1928–1932.
41 C. Byrne, L. Moran, D. Hermosilla, N. Merayo, Á. Blanco, S. Rhatigan, S. Hinder, P. Ganguly, M. Nolan and S. C. Pillai, Effect of Cu doping on the anatase-to-rutile phase transition in TiO_2 photocatalysts: Theory and experiments, *Appl. Catal., B*, 2019, **246**, 266–276.
42 T. Wang, G. Qu, J. Ren, Q. Sun, D. Liang and S. Hu, Organic acids enhanced decoloration of azo dye in gas phase surface discharge plasma system, *J. Hazard. Mater.*, 2016, **302**, 65–71.
43 A. S. Bansode, S. E. More, E. A. Siddiqui, S. Satpute, A. Ahmad, S. V. Bhoraskar and V. L. Mathe, Effective degradation of organic water pollutants by atmospheric non-thermal plasma torch and analysis of degradation process, *Chemosphere*, 2017, **167**, 396–405.
44 Y. S. Mok, J.-O. Jo and J. C. Whitehead, Degradation of an azo dye Orange II using a gas phase dielectric barrier discharge reactor submerged in water, *Chem. Eng. J.*, 2008, **142**, 56–64.
45 A. L. V. Cubas, M. de Medeiros Machado, J. R. dos Santos, J. J. Zanco, D. H. B. Ribeiro, A. S. André, N. A. Debacher and E. H. S. Moeck, Effect of chemical species generated by different geometries of air and argon non-thermal plasma reactors on bacteria inactivation in water, *Sep. Purif. Technol.*, 2019, **222**, 68–74.
46 H. Guo, N. Jiang, H. Wang, K. Shang, N. Lu, J. Li and Y. Wu, Enhanced catalytic performance of graphene-TiO_2 nanocomposites for synergetic degradation of fluoroquinolone antibiotic in pulsed discharge plasma system, *Appl. Catal., B*, 2019, **248**, 552–566.
47 A. Valério, J. Wang, S. Tong, A. A. U. de Souza, D. Hotza and S. Y. G. González, Synergetic effect of photocatalysis and ozonation for enhanced tetracycline degradation using highly macroporous photocatalytic supports, *Chem. Eng. Process.*, 2020, **149**, 107838.
48 M. Vijay, K. Ramachandran, P. V. Ananthapadmanabhan, B. Nalini, B. C. Pillai, F. Bondioli, A. Manivannan and R. T. Narendhirakannan, Photocatalytic inactivation of Gram-positive and Gram-negative bacteria by reactive plasma processed nanocrystalline TiO_2 powder, *Curr. Appl. Phys.*, 2013, **13**, 510–516.
49 Z. Huang, P. C. Maness, D. M. Blake, E. J. Wolfrum, S. L. Smolinski and W. A. Jacoby, Bactericidal mode of titanium dioxide photocatalysis, *J. Photochem. Photobiol., A*, 2000, **130**, 163.
50 C. S. Turchi and D. F. Ollis, Photocatalytic degradation of organic water contaminants: Mechanisms involving hydroxyl radical attack, *J. Catal.*, 1990, **122**, 178.
51 O. Legrini, E. Oliveros and M. A. Braun, Photochemical processes for water treatment, *Chem. Rev.*, 1993, **93**, 671.
52 B. Moongraksathum, J. Y. Shang and Y. W. Chen, Photocatalytic antibacterial effectiveness of Cu-doped TiO_2 thin film prepared *via* the peroxo sol-gel method, *Catalysts*, 2018, **8**, 352.
53 R. J. Wandell, H. Wang, R. K. M. Bulusu, R. O. Gallan and B. R. Locke, Formation of nitrogen oxides by nanosecond pulsed plasma discharges in gas–liquid reactors, *Plasma Chem. Plasma Process.*, 2019, **39**, 643–666.
54 T. Wang, G. Qu, J. Ren, Q. Sun, D. Liang and S. Hu, Organic acids enhanced decoloration of azo dye in gas phase surface discharge plasma system, *J. Hazard. Mater.*, 2016, **302**, 65–71.
55 P. Murugesan, J. A. Moses and C. Anandharamakrishnan, Performance of an atmospheric plasma discharge reactor for inactivation of Enterococcus faecalis and Escherichia coli in aqueous media, *J. Environ. Chem. Eng.*, 2020, 103891.
56 P. Sun, H. Wu, N. Bai, H. Zhou, R. Wang, H. g. Feng, W. Zhu, J. Zhang and J. Fang, Inactivation of Bacillus subtilis Spores in Water by a Direct-Current, Cold Atmospheric-Pressure Air Plasma Microjet, *Plasma Processes Polym.*, 2012, **9**, 157–164.
57 Z. Zhu, H. Cai and D. W. Sun, Titanium dioxide (TiO_2) photocatalysis technology for nonthermal inactivation of microorganisms in foods, *Trends Food Sci. Technol.*, 2018, **75**, 23–35.